SOI: 1.1/TAS DOI: 10.15863/TAS

International Scientific Journal

Theoretical & Applied Science

p-ISSN: 2308-4944 (print) **e-ISSN:** 2409-0085 (online)

Year: 2023 **Issue:** 12 **Volume:** 128

Published: 01.12.2023 http://T-Science.org

Issue Article

Denis Chemezov
Vladimir Industrial College
M.Sc.Eng., Honorary Worker of the Education Field of the Russian Federation, Academician of International Academy of Theoretical and Applied Sciences, Lecturer, Russian Federation
https://orcid.org/0000-0002-2747-552X
vic-science@yandex.ru

Pyotr German
Moscow Aviation Institute (NRU)
Branch in Zhukovsky, Moscow Oblast,
Student, Russian Federation

Aleksandr Zhirov
Vladimir Industrial College
Student, Russian Federation

Aleksey Fetisov
Vladimir Industrial College
Student, Russian Federation

Vitaliy Peskov
Vladimir Industrial College
Student, Russian Federation

Vladislav Samoylov
Vladimir Industrial College
Student, Russian Federation

Abubakr Khasanov
Vladimir Industrial College
Student, Russian Federation

REFERENCE DATA OF PRESSURE DISTRIBUTION ON THE SURFACES OF AIRFOILS HAVING THE NAMES BEGINNING WITH THE LETTER W

Abstract: *The results of the computer calculation of air flow around the airfoils having the names beginning with the letter W are presented in the article. The contours of pressure distribution on the surfaces of the airfoils at angles of attack of 0, 15 and -15 degrees in conditions of the subsonic airplane flight speed were obtained.*

Key words: *airfoil, angle of attack, pressure, surface.*

Language: *English*

Citation: Chemezov, D., et al. (2023). Reference data of pressure distribution on the surfaces of airfoils having the names beginning with the letter W. *ISJ Theoretical & Applied Science, 12 (128),* 1-27.

Soi: http://s-o-i.org/1.1/TAS-12-128-1 ***Doi***: crossref https://dx.doi.org/10.15863/TAS.2023.12.128.1

Scopus ASCC: *1507.*

Introduction

Creating reference materials that determine the most accurate pressure distribution on the airfoil surfaces is an actual task of the airplane aerodynamics.

Materials and methods

The study of air flow around the airfoils was carried out in a two-dimensional formulation by means of the computer calculation in the *Comsol Multiphysics* program. The airfoils in the cross section were taken as objects of research [1-39]. In this work, the airfoils having the names beginning with the letter *W* were adopted. Air flow around the airfoils was carried out at angles of attack (α) of 0, 15 and -15 degrees. Flight speed of the airplane in each case was subsonic. The airplane flight in the atmosphere was carried out under normal weather conditions. The geometric characteristics of the studied airfoils are presented in the Table 1. The geometric shapes of the airfoils in the cross section are presented in the Table 2.

Table 1. The geometric characteristics of the airfoils.

Airfoil name	Max. thickness	Max. camber	Leading edge radius	Trailing edge thickness
WACO COOTIE	8.46% at 30.0% of the chord	6.28% at 40.0% of the chord	0.8839%	0.5%
WASP (smoothed)	9.35% at 27.1% of the chord	2.98% at 37.9% of the chord	0.794%	0.023%
WB-135-35 13,5% smoothed	13.55% at 25.0% of the chord	3.75% at 50.0% of the chord	1.0142%	0.0%
WB-140-35-FB 14%	13.93% at 35.0% of the chord	3.7% at 45.0% of the chord	1.096%	0.5%
Westphal 18105	10.5% at 30.0% of the chord	1.75% at 30.0% of the chord	1.7056%	0.2%
WHITCOMB INTEGRAL SUPERCRITICAL	10.96% at 35.0% of the chord	2.29% at 82.5% of the chord	1.9733%	0.05%
WOODSTOK	5.7% at 20.0% of the chord	7.85% at 50.0% of the chord	1.3239%	0.3%
WORTMANN FX 049-915	14.72% at 37.1% of the chord	5.82% at 37.1% of the chord	1.4886%	0.0%
WORTMANN FX 05-188	18.82% at 37.1% of the chord	2.62% at 50.0% of the chord	1.6214%	0.0%
WORTMANN FX 05-191	19.08% at 37.1% of the chord	2.62% at 50.0% of the chord	1.3765%	0.0%
WORTMANN FX 057-816	16.18% at 37.1% of the chord	5.13% at 37.1% of the chord	1.5276%	0.0%
WORTMANN FX 05-H-126	12.61% at 37.1% of the chord	4.4% at 37.1% of the chord	0.8007%	0.0%
WORTMANN FX 082-512	11.8% at 25.0% of the chord	4.16% at 62.9% of the chord	1.2991%	0.0%
WORTMANN FX 08-S-176	17.61% at 37.1% of the chord	5.66% at 37.1% of the chord	0.6544%	0.0%
WORTMANN FX 2	20.45% at 43.5% of the chord	3.77% at 69.1% of the chord	1.601%	0.0%
WORTMANN FX 3	19.98% at 50.0% of the chord	4.16% at 75.0% of the chord	1.5151%	0.0%
WORTMANN FX 60-126	12.59% at 27.9% of the chord	3.56% at 56.5% of the chord	1.0934%	0.0%
WORTMANN FX 60-126-1	12.58% at 30.0% of the chord	3.93% at 50.0% of the chord	1.2355%	0.0%
WORTMANN FX 61-140	14.0% at 30.0% of the chord	2.4% at 30.0% of the chord	1.2795%	0.0%
WORTMANN FX 62-K-131	13.09% at 40.2% of the chord	3.89% at 53.3% of the chord	0.5774%	0.0%
WORTMANN FX 62-K-131-17	13.16% at 40.0% of the chord	3.92% at 50.0% of the chord	0.903%	0.0%
WORTMANN FX 63-100	10.1% at 30.0% of the chord	4.34% at 50.0% of the chord	1.1317%	0.0%
WORTMANN FX 63-120	12.0% at 30.0% of the chord	5.31% at 60.0% of the chord	1.2814%	0.0%
WORTMANN FX 63-137	13.71% at 30.9% of the chord	5.97% at 53.3% of the chord	1.336%	0.0%
WORTMANN FX 66-17A-175	17.52% at 33.9% of the chord	4.16% at 40.2% of the chord	0.581%	0.0%
WORTMANN FX 66-17AII-182	18.84% at 35.0% of the chord	3.65% at 40.1% of the chord	0.9998%	0.08%
WORTMANN FX 71-089A	8.94% at 22.2% of the chord	0.0% at 0.0% of the chord	1.6569%	0.0%
WORTMANN FX 71-120	11.99% at 25.0% of the chord	0.0% at 0.0% of the chord	2.2348%	0.0%
WORTMANN FX 72-MS-150A	15.01% at 37.1% of the chord	8.34% at 46.7% of the chord	1.6172%	0.0%
WORTMANN FX 72-MS-150B	15.01% at 37.1% of the chord	9.72% at 46.7% of the chord	1.498%	0.0%
Wortmann FX 74-CL5-140 Modified	13.08% at 27.1% of the chord	9.72% at 41.6% of the chord	0.985%	0.012%
WORTMANN FX 77-W-153	15.26% at 27.9% of the chord	4.49% at 27.9% of the chord	1.5674%	0.181%
WORTMANN FX 77-W-258	26.15% at 30.9% of the chord	4.34% at 27.9% of the chord	7.0492%	1.219%
WORTMANN FX 77-W-343	34.41% at 34.0% of the chord	4.7% at 25.0% of the chord	11.4941%	4.223%
WORTMANN FX 79-K-144-17	14.39% at 43.5% of the chord	2.81% at 40.2% of the chord	0.9631%	0.2%
WORTMANN FX L V-152	15.3% at 34.0% of the chord	0.0% at 0.0% of the chord	0.9243%	0.04%
WORTMANN FX M2	8.4% at 19.6% of the chord	4.78% at 30.9% of the chord	1.5513%	0.0%
WORTMANN FX-L-142-25	14.16% at 30.0% of the chord	0.0% at 0.0% of the chord	1.2879%	0.0%
WORTMANN M 2	8.23% at 20.0% of the chord	4.74% at 30.0% of the chord	1.3547%	0.25%
WRIGHT-6	13.6% at 30.0% of the chord	7.17% at 30.0% of the chord	1.5465%	0.0%
WRIGHTT1	13.37% at 30.0% of the chord	7.06% at 40.0% of the chord	1.7369%	0.21%
Note: *Westphal 18105 (F. Westphal (Germany)), Wortmann FX 74-CL5-140 Modified (high lift airfoil).*				

Table 2. The geometric shapes of the airfoils in the cross section.

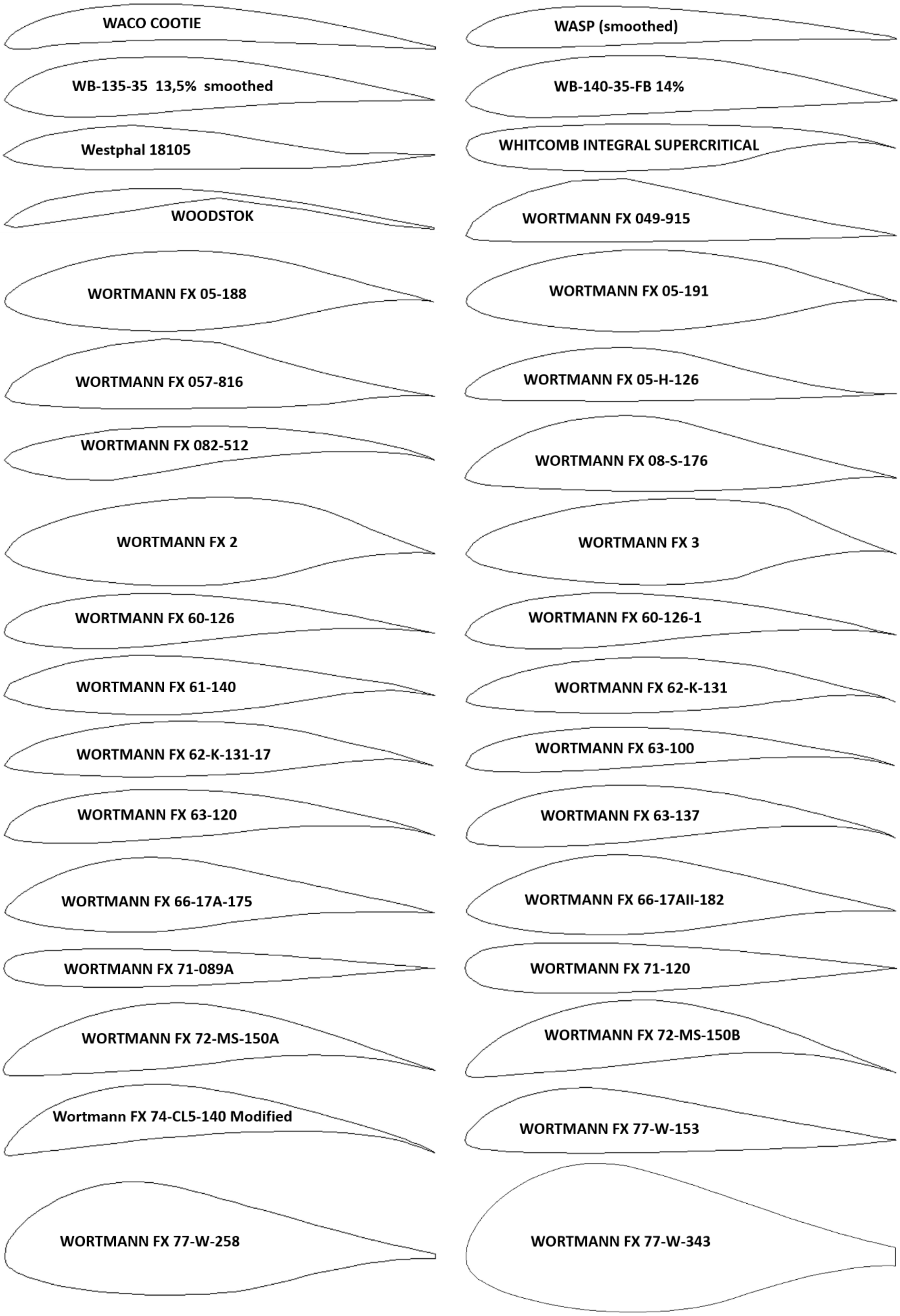

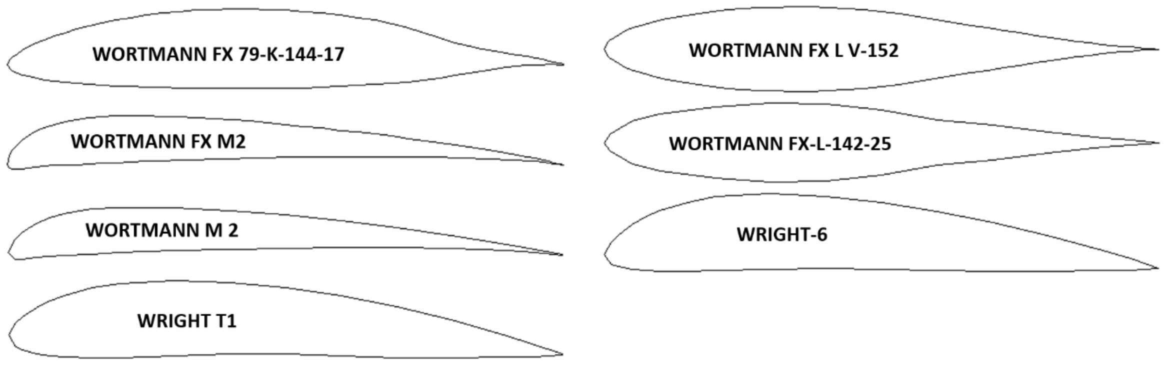

Results and discussion

The calculated pressure contours on the surfaces of the airfoils at different angles of attack are presented in the Figs. 1-41. The calculated values on the scale can be represented as the basic values when comparing the pressure drop under conditions of changing the angle of attack of the airfoils.

41 WORTMANN type airfoils and a number of others were considered. All airfoils are asymmetrical, with the exception of WORTMANN FX 71-089A, WORTMANN FX 71-120, WORTMANN FX L V-152 and WORTMANN FX-L-142-25.

The WORTMANN FX 77-W-343 airfoil has a maximum thickness of 34.41%. The minimum thickness of 5.7% is determined for the WOODSTOK airfoil. The maximum camber of 9.72% is determined for the WORTMANN FX 72-MS-150B and Wortmann FX 74-CL5-140 Modified airfoils. The minimum camber of 0.0% is defined for the asymmetric airfoils. The largest leading edge radius of 11.4941% was noted for the WORTMANN FX 77-W-343 airfoil, and the minimum radius of 0.5774% was noted for the WORTMANN FX 62-K-131 airfoil. The largest thickening of the trailing edge of 4.223% was performed in the WORTMANN FX 77-W-343 airfoil. There is no thickening on the trailing edge for most airfoils.

Let us consider the aerodynamic characteristics of the airfoils described above.

Due to the curved geometric shape of the WOODSTOK airfoil, the pressure drop (positive and negative) on the upper and lower surfaces is negligible when the airplane descent. However, during the airplane climb on the leading edge of the airfoil, significant negative pressures arise, causing a large drag. The concave lower surface of the airfoil contributes to the formation of gradients of both positive and negative pressures.

The convex upper and lower surfaces of the WORTMANN FX 62-K-131 airfoil, when the airplane climb, lead to an increase in the drag on the leading edge, compared with the WOODSTOK airfoil. The airplane descent at an angle of attack of -15 degrees leads to a 3-fold pressure difference on the surfaces of the WORTMANN FX 62-K-131 airfoil.

The pressure drop on the surfaces of the WORTMANN FX 72-MS-150B airfoil during horizontal flight and descent of the airplane is almost the same. When climb, the pressure difference reaches a value of 2.5 times, which is the minimum value of the above-considered airfoils.

However, a similar configuration of the Wortmann FX 74-CL5-140 Modified airfoil, but with a smaller thickness, increases the pressure difference on the upper and lower surfaces by almost 2 times.

The WORTMANN FX 77-W-343 airfoil ensures the same pressure difference on the upper and lower surfaces during horizontal flight and climb of the airplane. The airplane descent with this airfoil of the wing leads to an increase in the drag by 2.5 times, compared with the airplane climb.

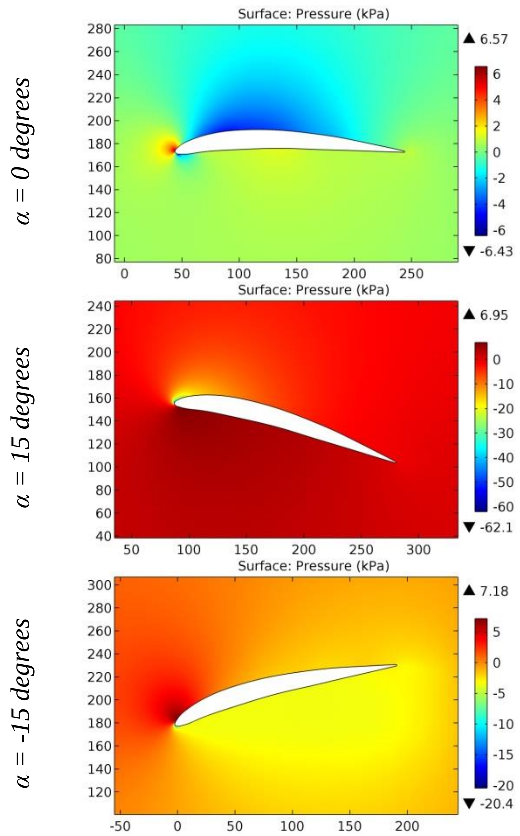

Figure 1. The pressure contours on the surfaces of the WACO COOTIE airfoil.

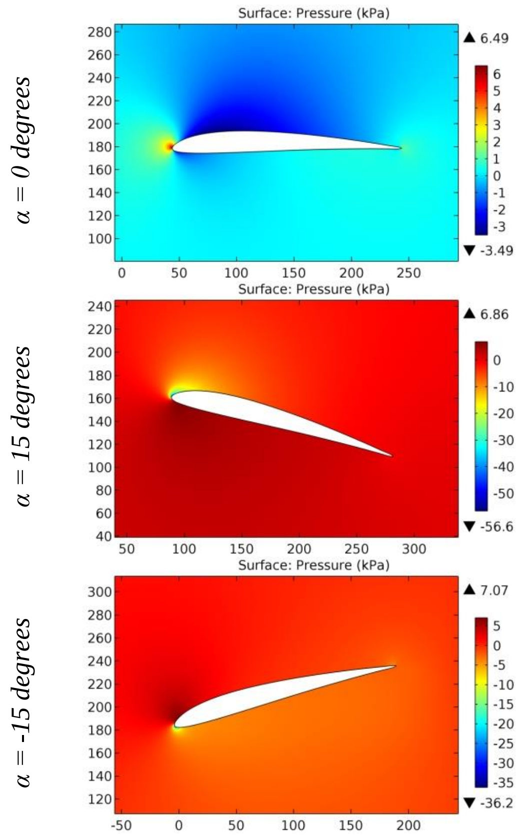

Figure 2. The pressure contours on the surfaces of the WASP (smoothed) airfoil.

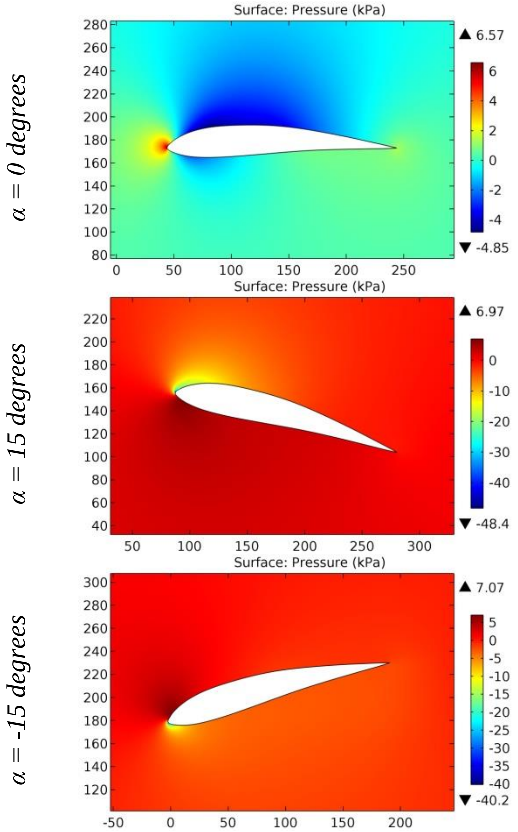

Figure 3. The pressure contours on the surfaces of the WB-135-35 13,5% smoothed airfoil.

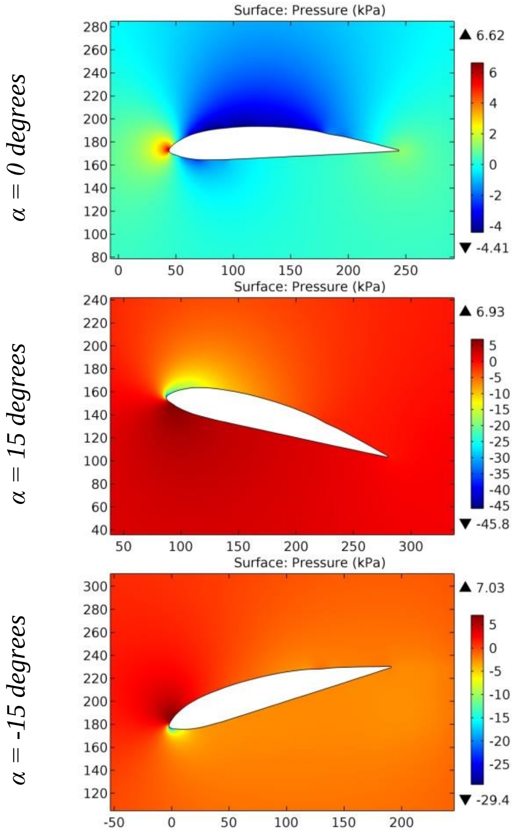

Figure 4. The pressure contours on the surfaces of the WB-140-35-FB 14% airfoil.

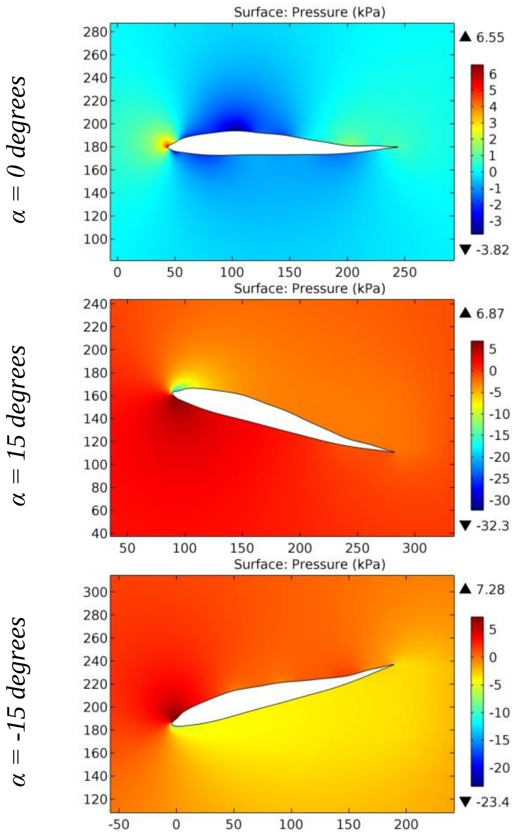

Figure 5. The pressure contours on the surfaces of the Westphal 18105 airfoil.

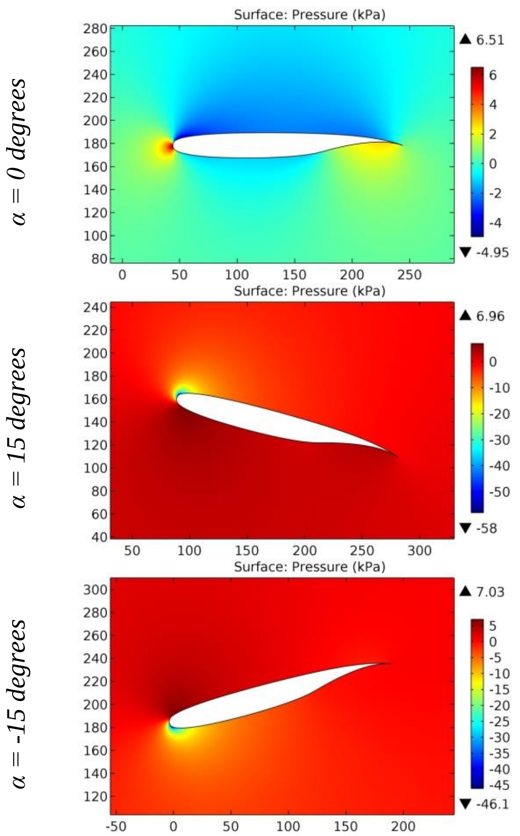

Figure 6. The pressure contours on the surfaces of the WHITCOMB INTEGRAL SUPERCRITICAL airfoil.

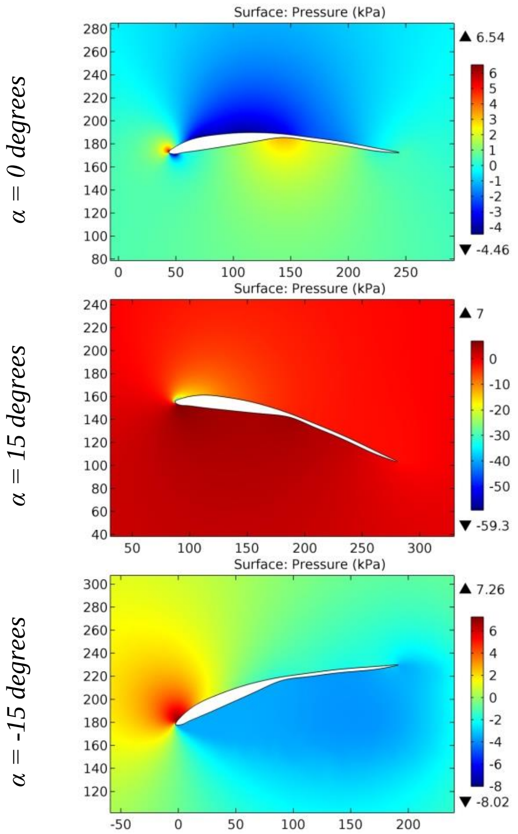

Figure 7. The pressure contours on the surfaces of the WOODSTOK airfoil.

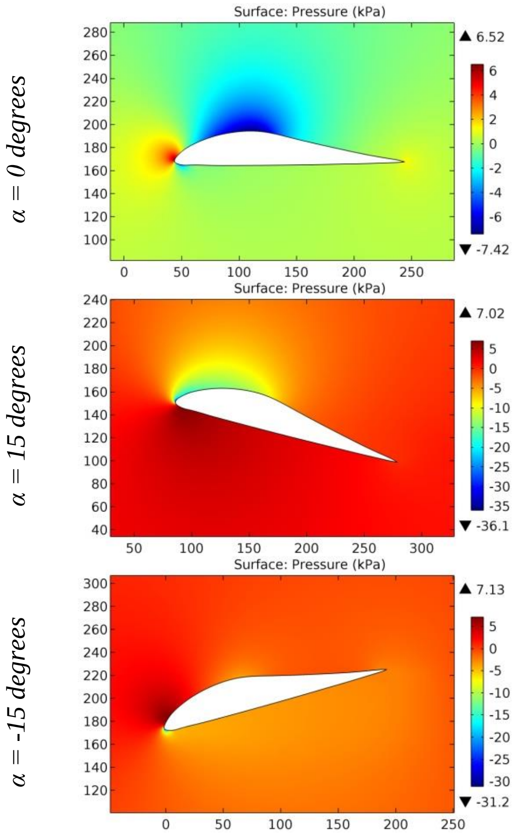

Figure 8. The pressure contours on the surfaces of the WORTMANN FX 049-915 airfoil.

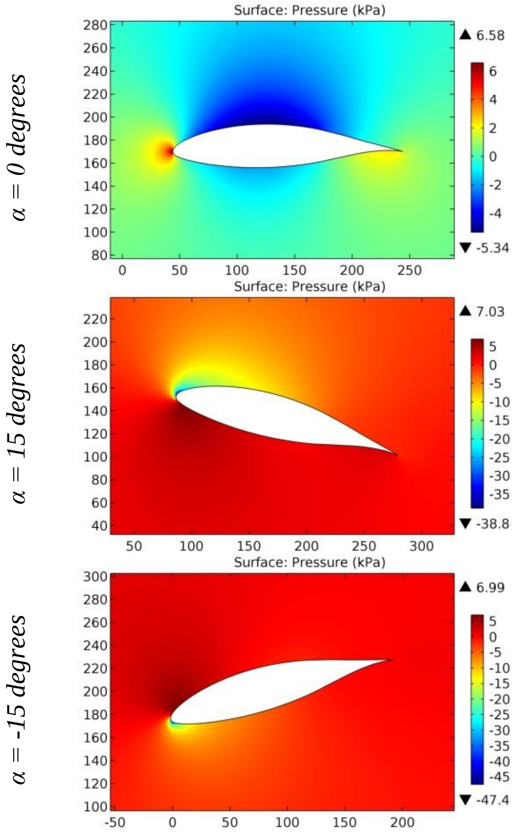

Figure 9. The pressure contours on the surfaces of the WORTMANN FX 05-188 airfoil.

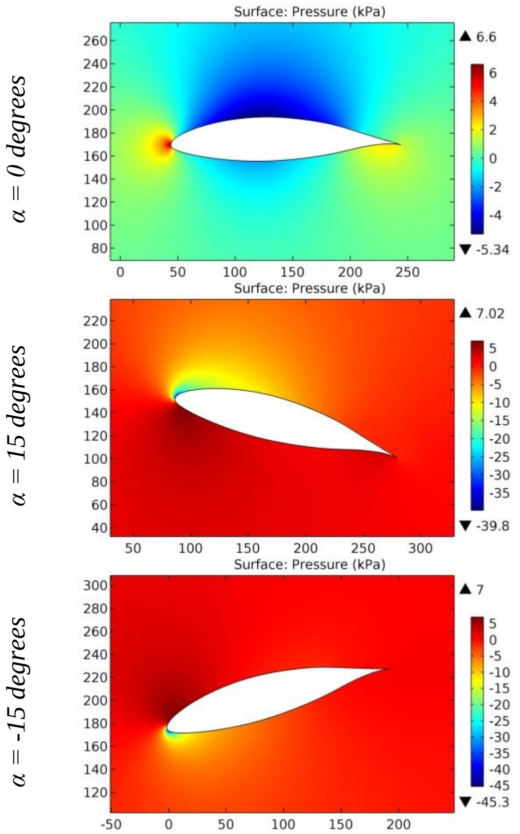

Figure 10. The pressure contours on the surfaces of the WORTMANN FX 05-191 airfoil.

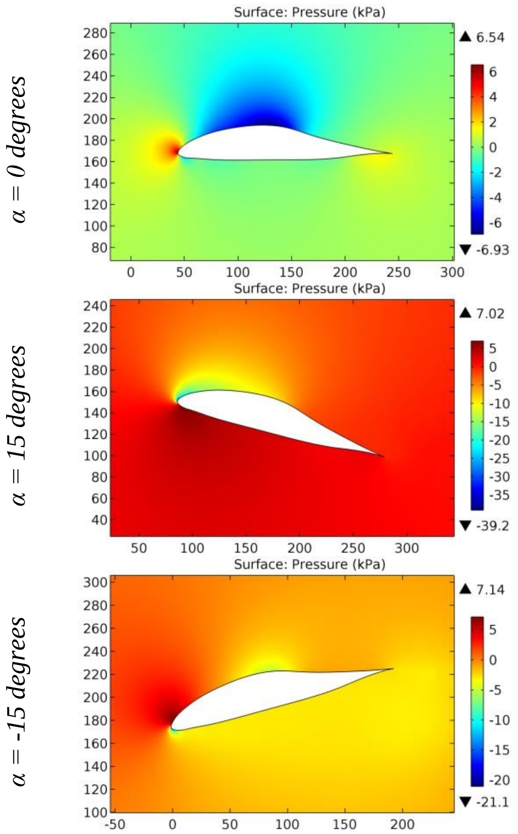

Figure 11. The pressure contours on the surfaces of the WORTMANN FX 057-816 airfoil.

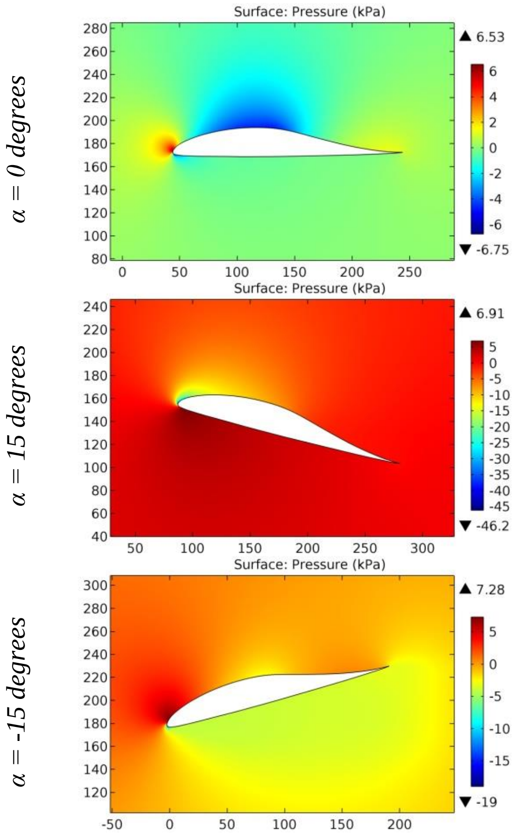

Figure 12. The pressure contours on the surfaces of the WORTMANN FX 05-H-126 airfoil.

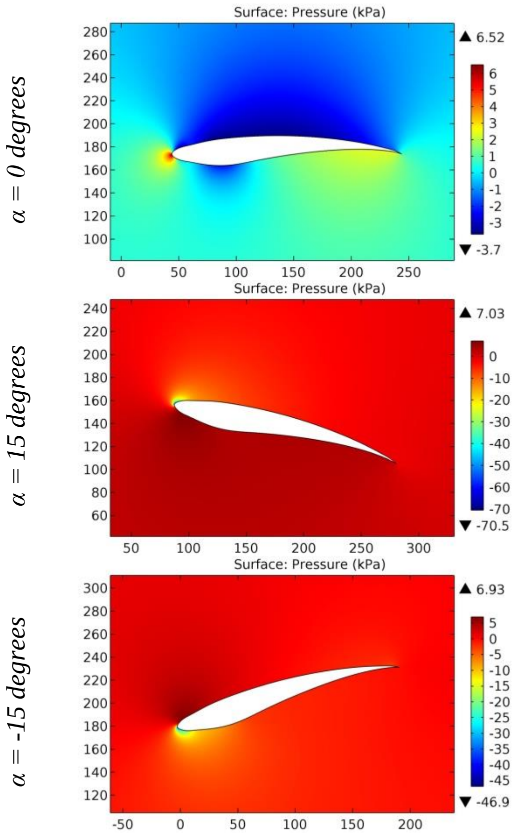

Figure 13. The pressure contours on the surfaces of the WORTMANN FX 082-512 airfoil.

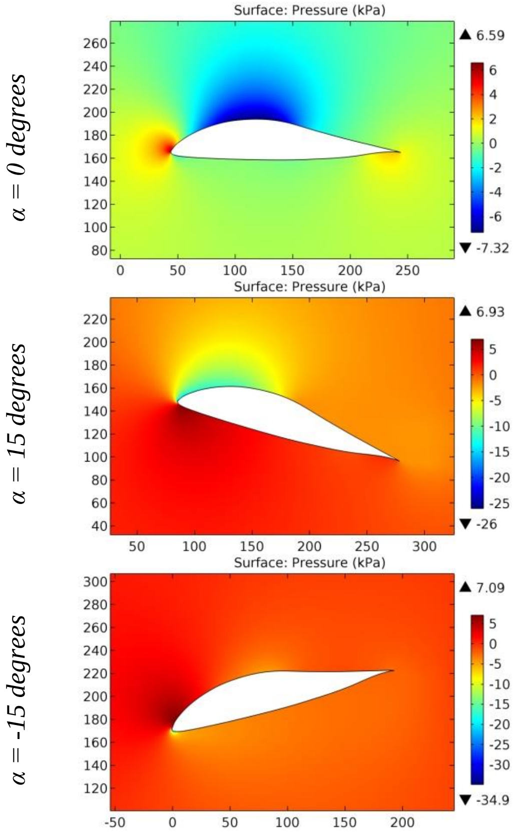

Figure 14. The pressure contours on the surfaces of the WORTMANN FX 08-S-176 airfoil.

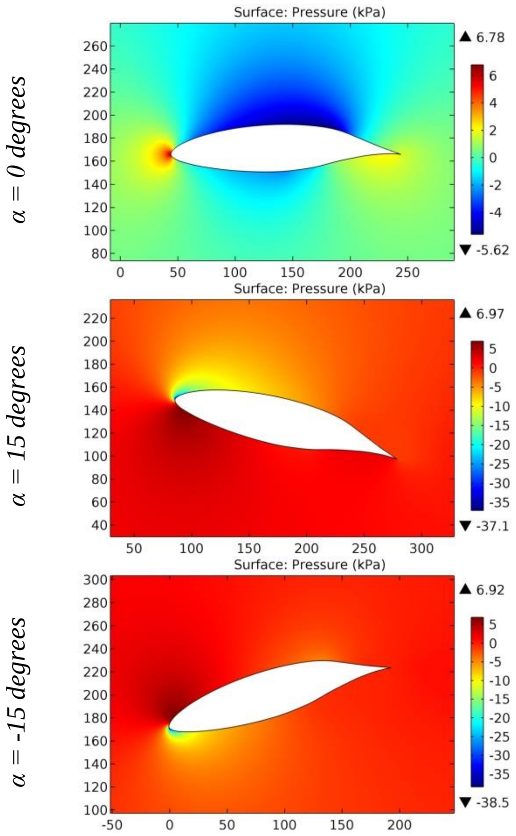

Figure 15. The pressure contours on the surfaces of the WORTMANN FX 2 airfoil.

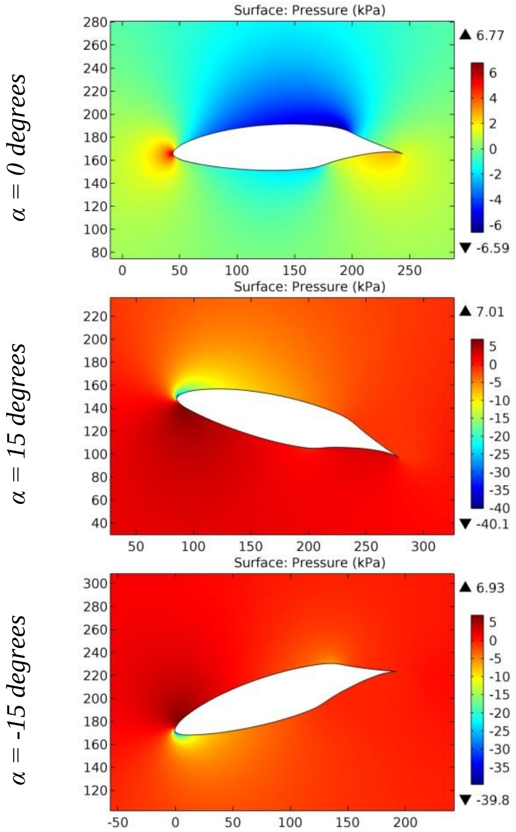

Figure 16. The pressure contours on the surfaces of the WORTMANN FX 3 airfoil.

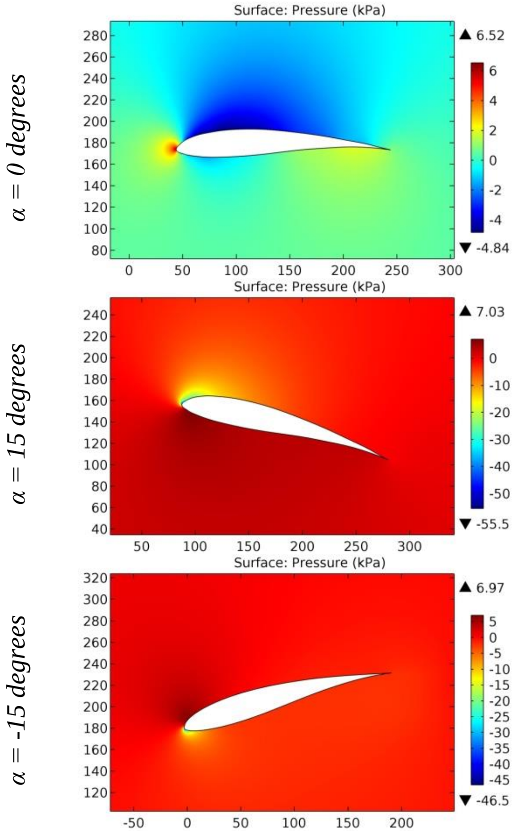

Figure 17. The pressure contours on the surfaces of the WORTMANN FX 60-126 airfoil.

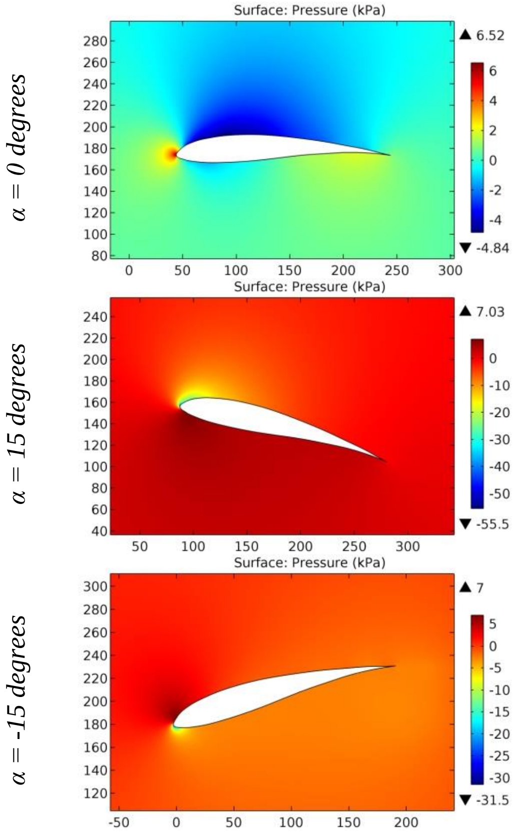

Figure 18. The pressure contours on the surfaces of the WORTMANN FX 60-126-1 airfoil.

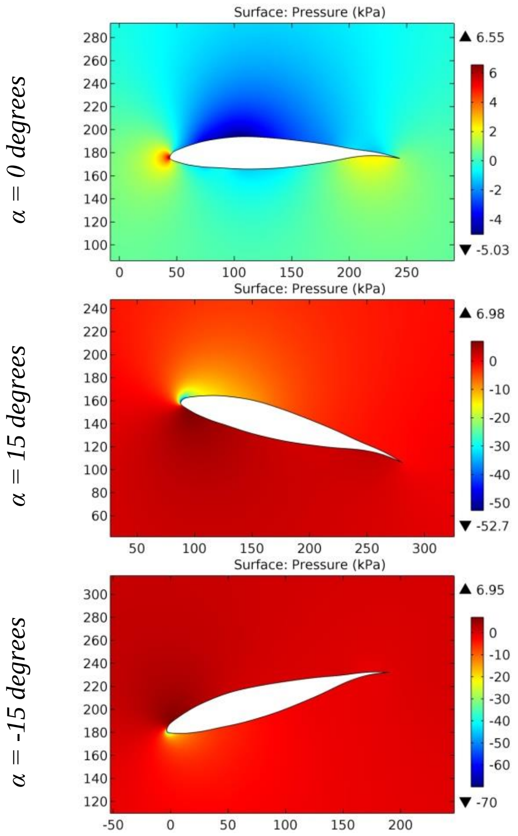

Figure 19. The pressure contours on the surfaces of the WORTMANN FX 61-140 airfoil.

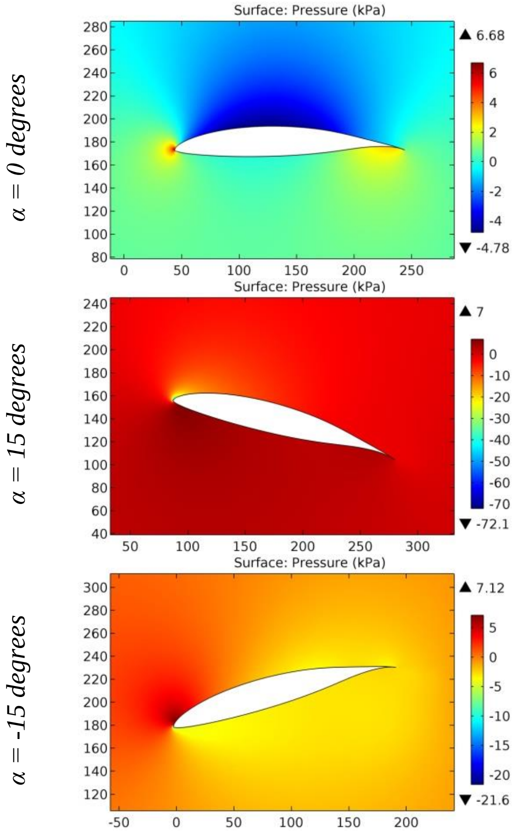

Figure 20. The pressure contours on the surfaces of the WORTMANN FX 62-K-131 airfoil.

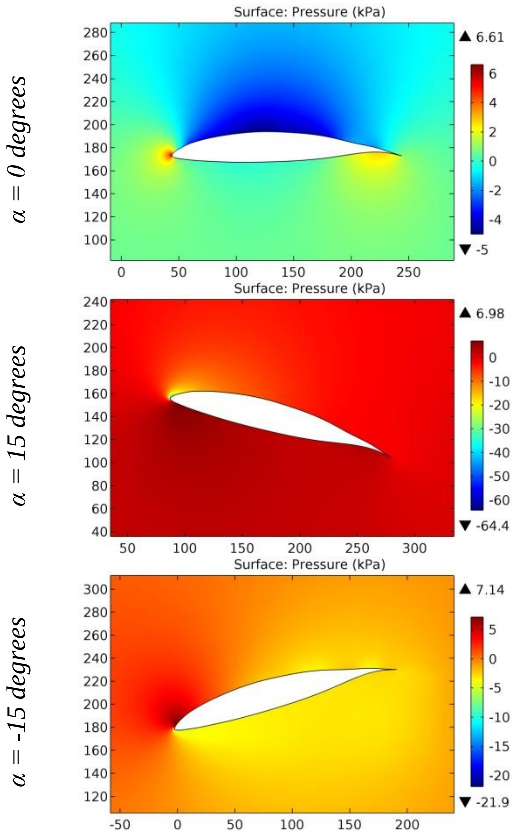

Figure 21. The pressure contours on the surfaces of the WORTMANN FX 62-K-131-17 airfoil.

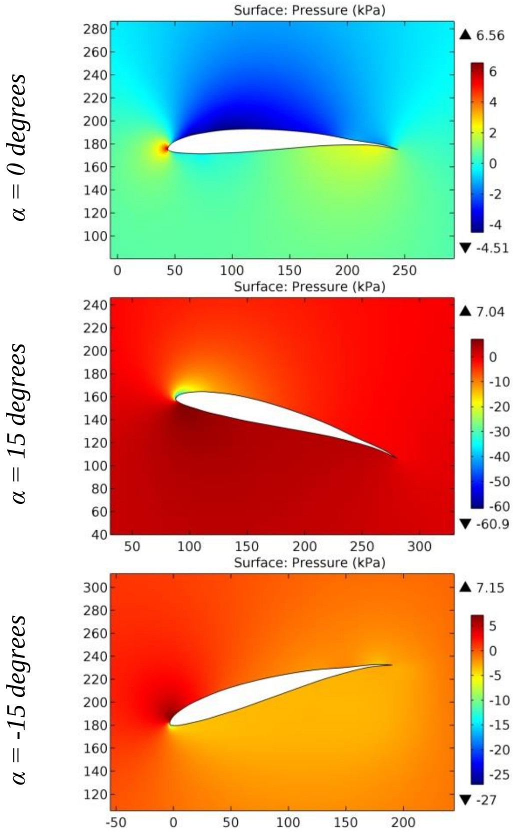

Figure 22. The pressure contours on the surfaces of the WORTMANN FX 63-100 airfoil.

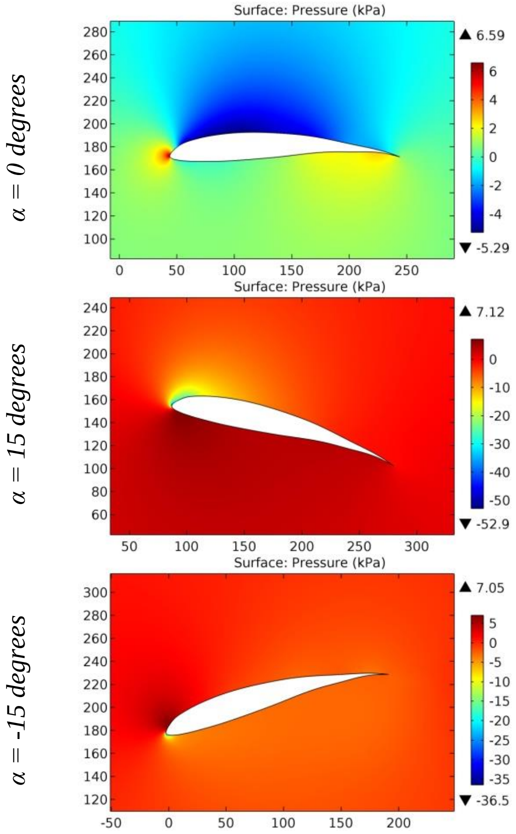

Figure 23. The pressure contours on the surfaces of the WORTMANN FX 63-120 airfoil.

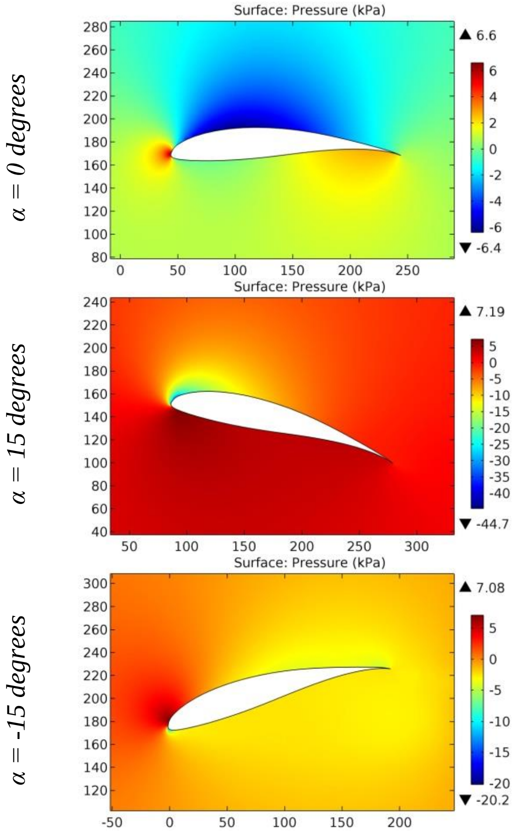

Figure 24. The pressure contours on the surfaces of the WORTMANN FX 63-137 airfoil.

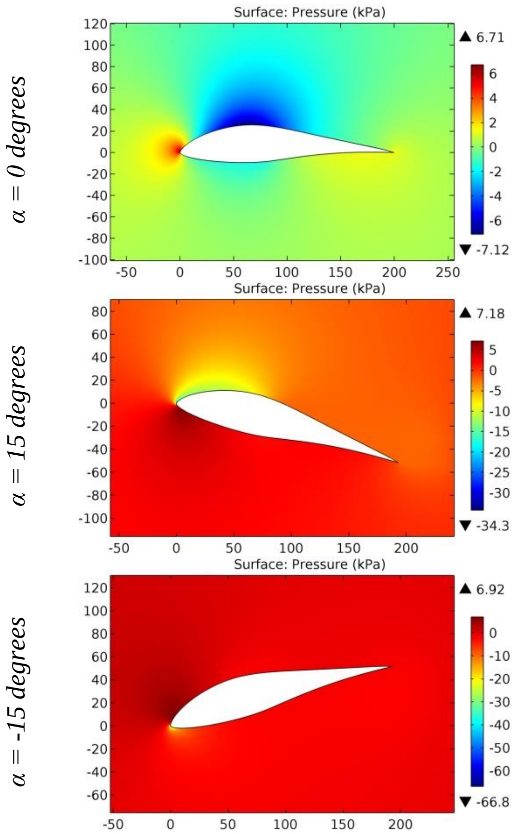

Figure 25. The pressure contours on the surfaces of the WORTMANN FX 66-17A-175 airfoil.

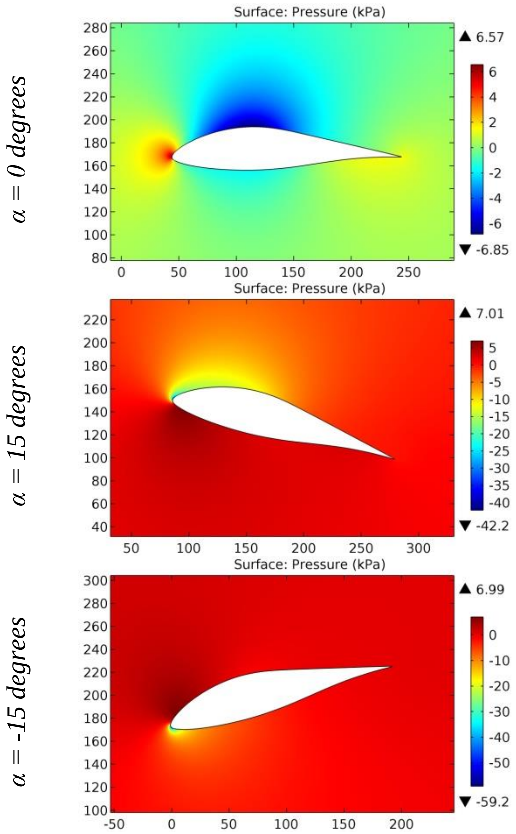

Figure 26. The pressure contours on the surfaces of the WORTMANN FX 66-17AII-182 airfoil.

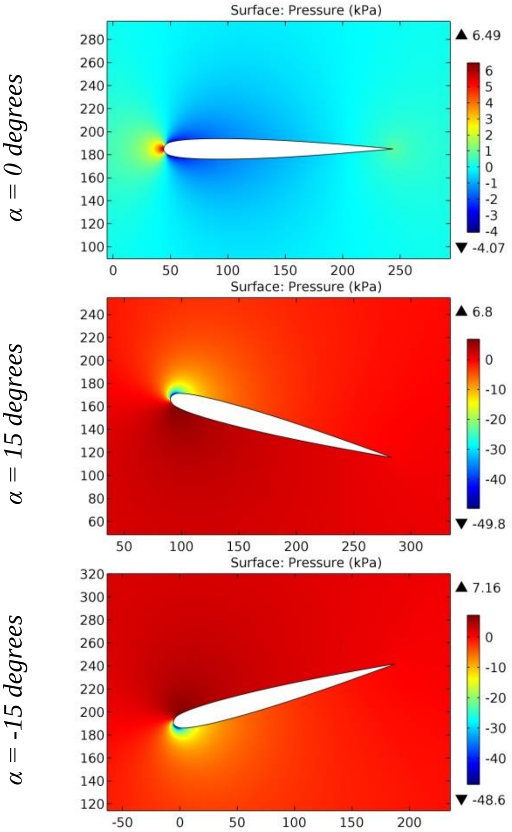

Figure 27. The pressure contours on the surfaces of the WORTMANN FX 71-089A airfoil.

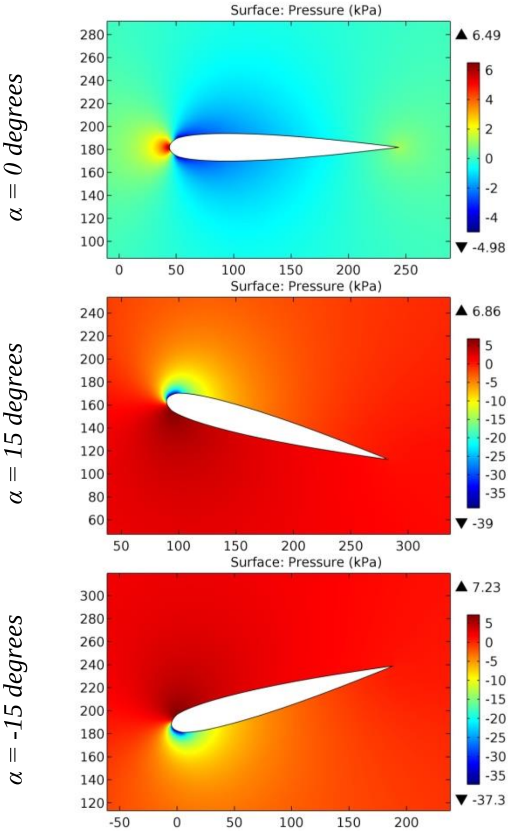

Figure 28. The pressure contours on the surfaces of the WORTMANN FX 71-120 airfoil.

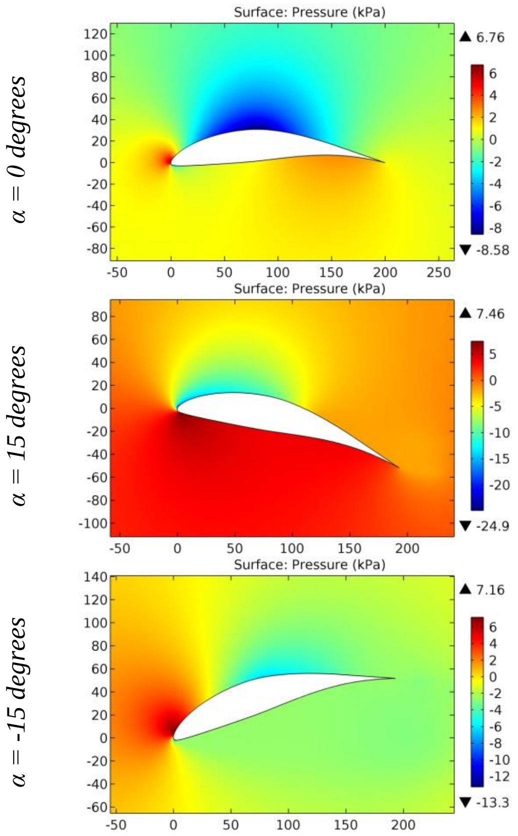

Figure 29. The pressure contours on the surfaces of the WORTMANN FX 72-MS-150A airfoil.

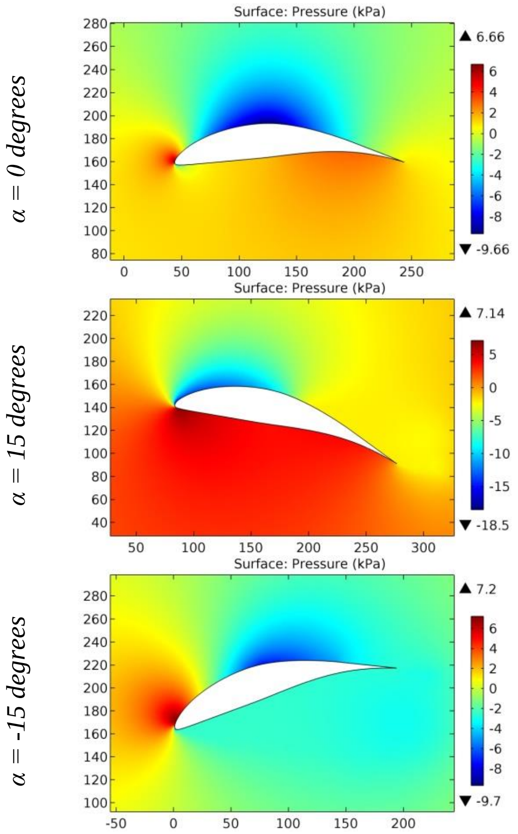

Figure 30. The pressure contours on the surfaces of the WORTMANN FX 72-MS-150B airfoil.

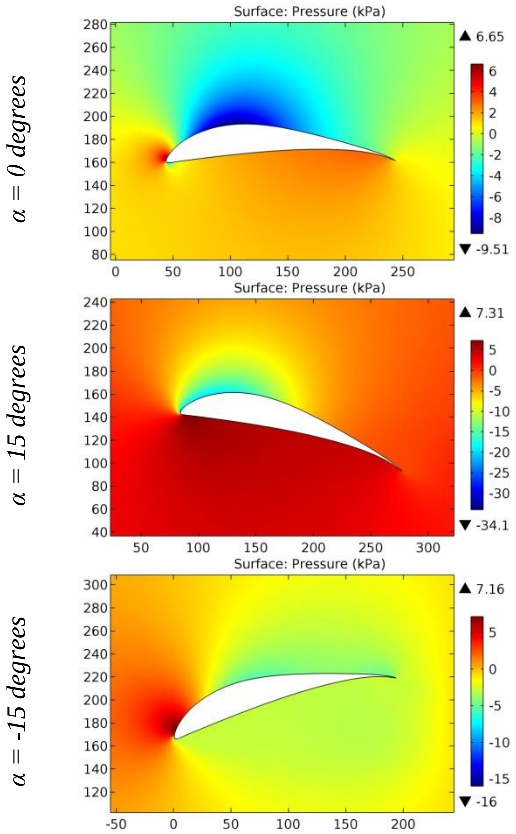

Figure 31. The pressure contours on the surfaces of the Wortmann FX 74-CL5-140 Modified airfoil.

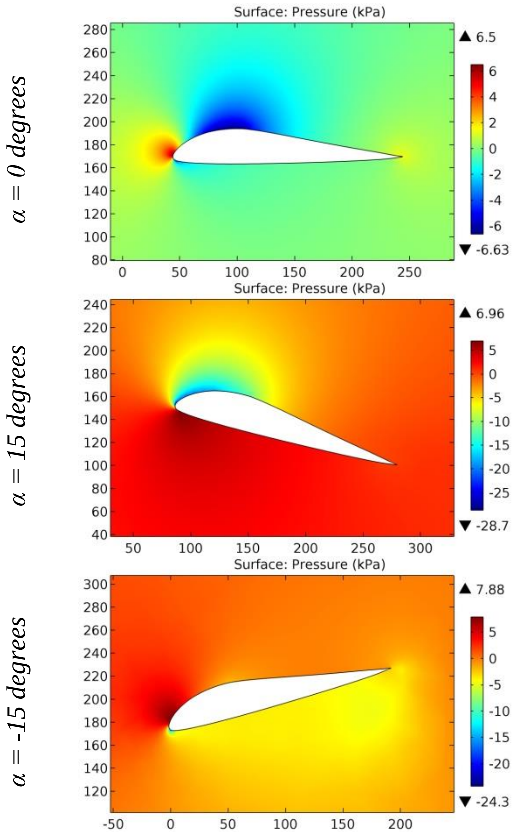

Figure 32. The pressure contours on the surfaces of the WORTMANN FX 77-W-153 airfoil.

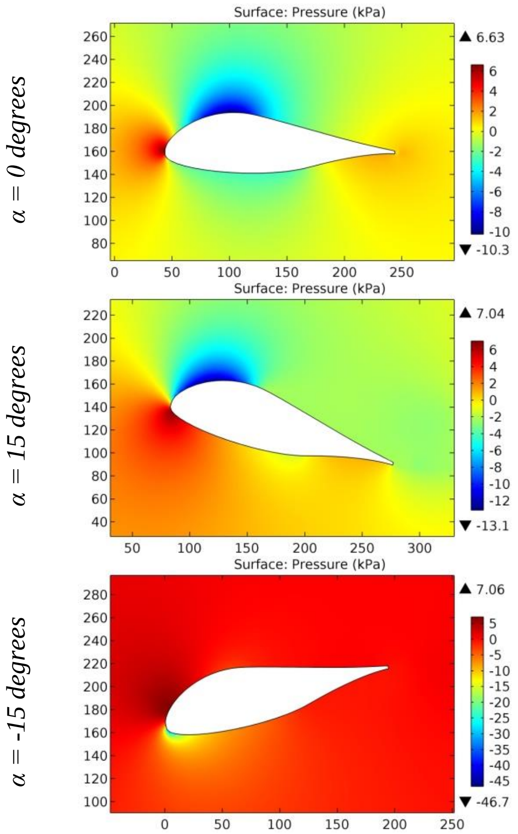

Figure 33. The pressure contours on the surfaces of the WORTMANN FX 77-W-258 airfoil.

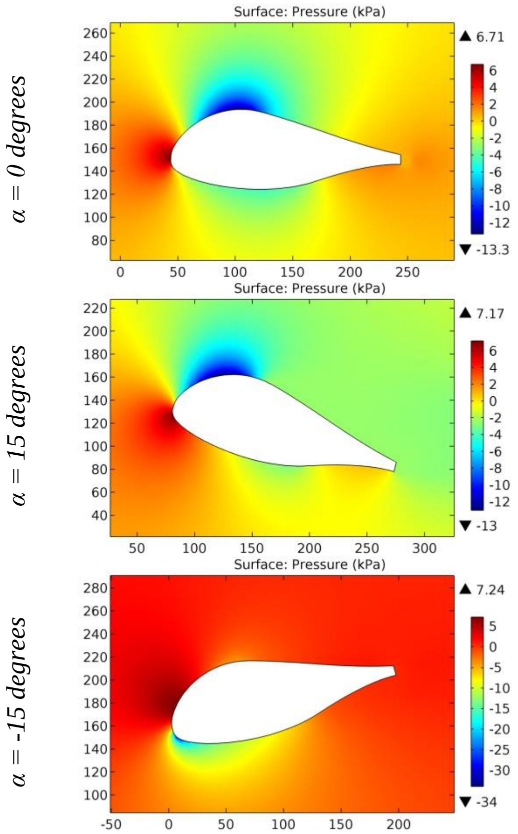

Figure 34. The pressure contours on the surfaces of the WORTMANN FX 77-W-343 airfoil.

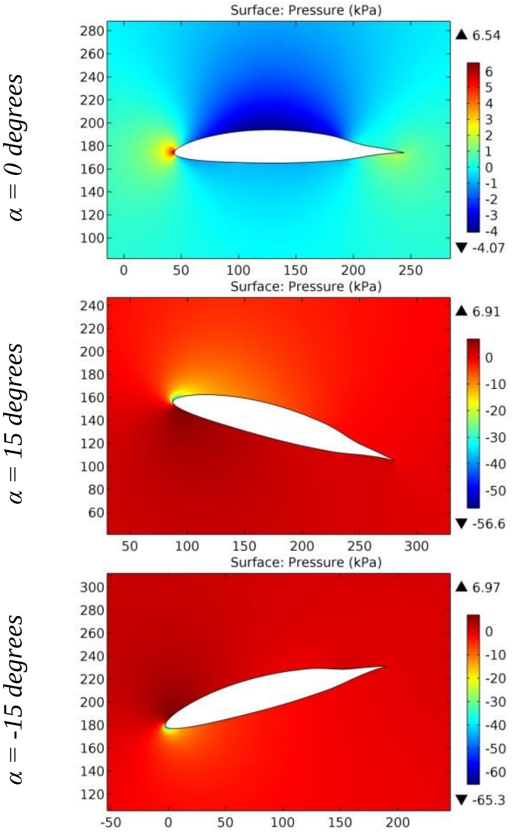

Figure 35. The pressure contours on the surfaces of the WORTMANN FX 79-K-144-17 airfoil.

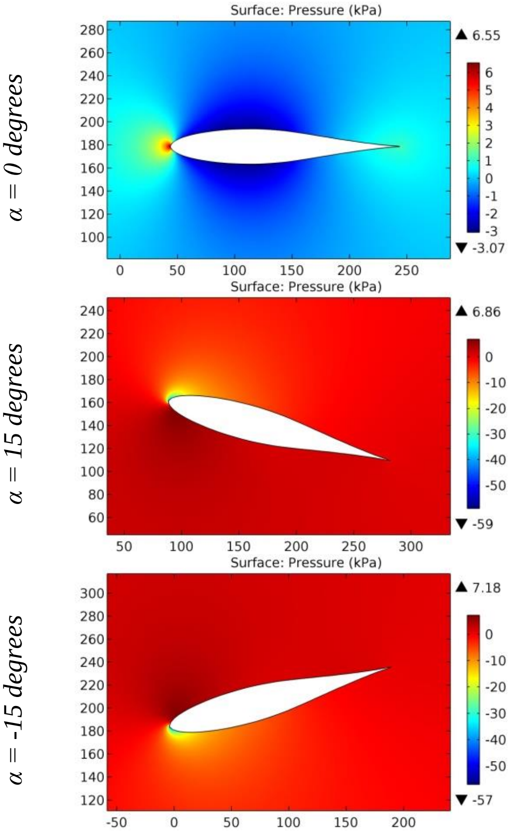

Figure 36. The pressure contours on the surfaces of the WORTMANN FX L V-152 airfoil.

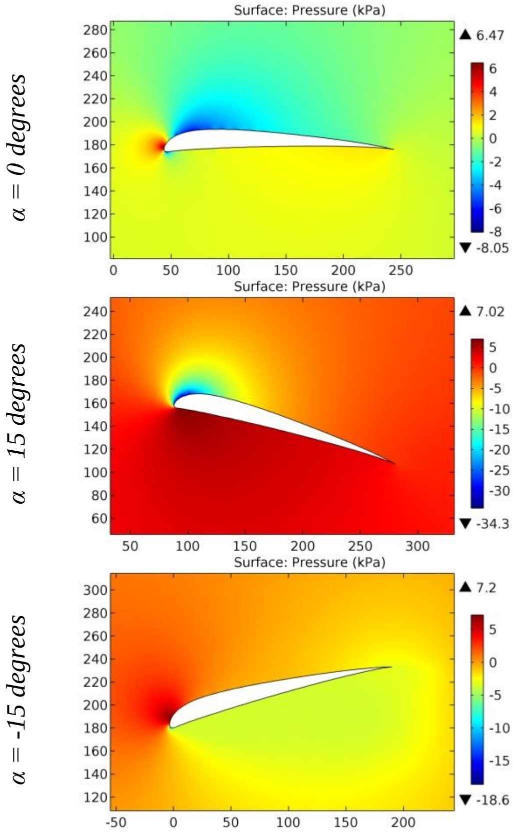

Figure 37. The pressure contours on the surfaces of the WORTMANN FX M2 airfoil.

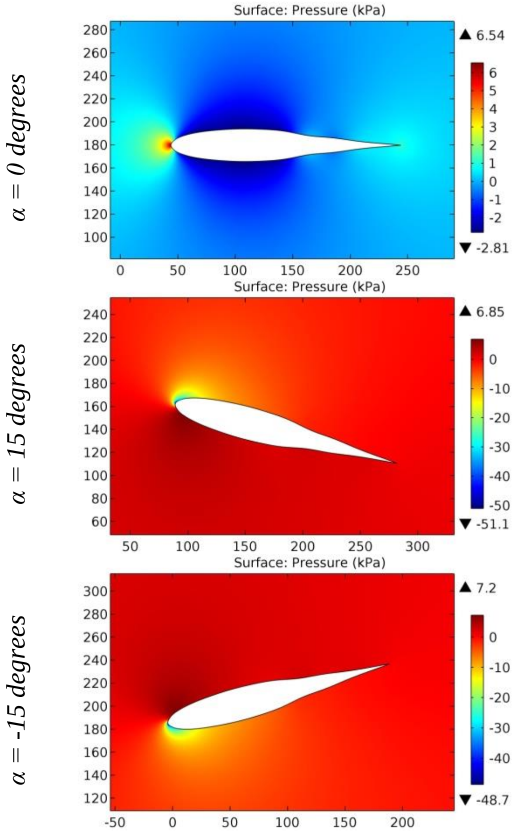

Figure 38. The pressure contours on the surfaces of the WORTMANN FX-L-142-25 airfoil.

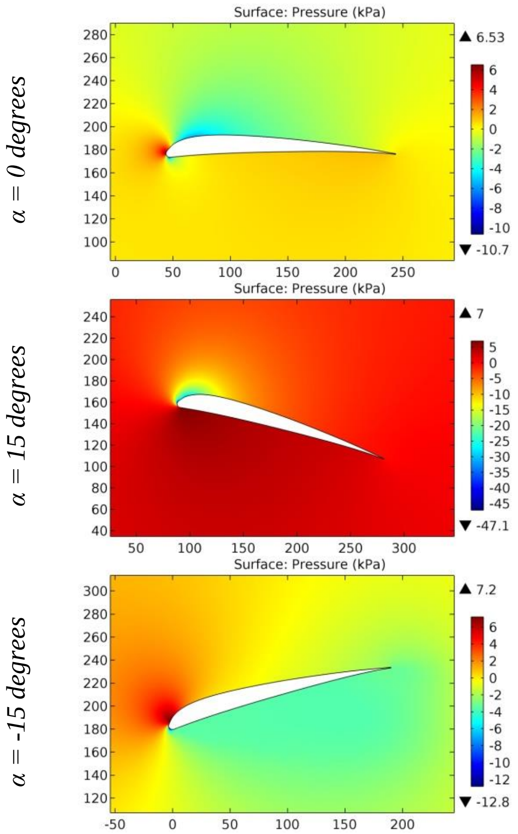

Figure 39. The pressure contours on the surfaces of the WORTMANN M 2 airfoil.

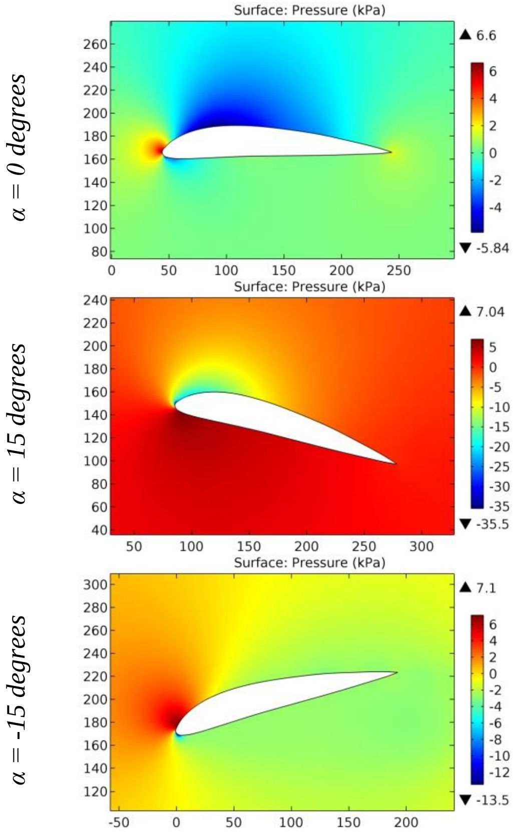

Figure 40. The pressure contours on the surfaces of the WRIGHT-6 airfoil.

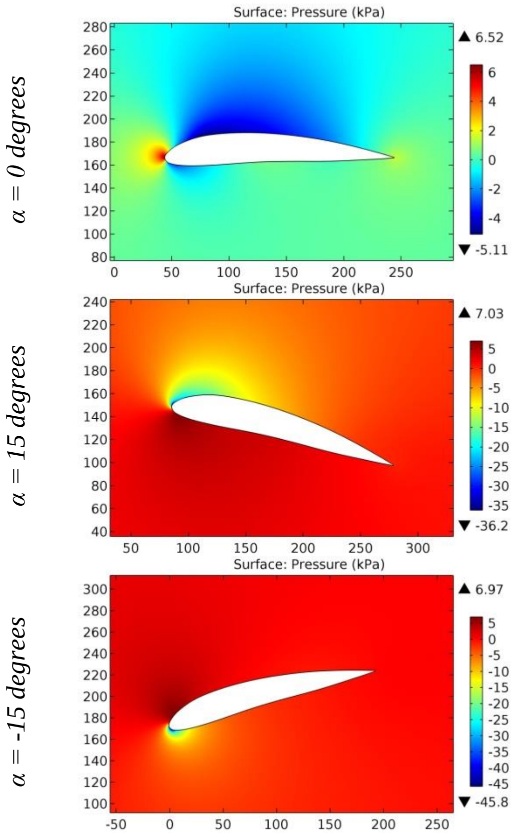

Figure 41. The pressure contours on the surfaces of the WRIGHT T1 airfoil.

Conclusion

The reduction of drag on the surfaces of the airplane wings can be provided by a rational configuration of the airfoil. To search for and further select airfoils with the best aerodynamic characteristics, computer testing of configurations of the airplane wing elements in cross section is proposed, taking into account the use of real boundary conditions, turbulence models, etc. For horizontal flight and the main maneuvers of the airplane, the dependences of the change in the value of drag and lift on the thickness, camber, radius of the leading edge and thickness of the trailing edge of the airfoil were determined. Thus, the time of testing the configuration of the airfoil is reduced with the possibility of obtaining reliable results at the design stage of the airplane wing.

References:

1. Anderson, J. D. (2010). *Fundamentals of Aerodynamics*. McGraw-Hill, Fifth edition.
2. Shevell, R. S. (1989). *Fundamentals of Flight*. Prentice Hall, Second edition.
3. Houghton, E. L., & Carpenter, P. W. (2003). *Aerodynamics for Engineering Students*. Fifth edition, Elsevier.
4. Lan, E. C. T., & Roskam, J. (2003). *Airplane Aerodynamics and Performance*. DAR Corp.
5. Sadraey, M. (2009). *Aircraft Performance Analysis*. VDM Verlag Dr. Müller.
6. Anderson, J. D. (1999). *Aircraft Performance and Design*. McGraw-Hill.
7. Roskam, J. (2007). *Airplane Flight Dynamics and Automatic Flight Control*, Part I. DAR Corp.
8. Etkin, B., & Reid, L. D. (1996). *Dynamics of Flight, Stability and Control*. Third Edition, Wiley.
9. Stevens, B. L., & Lewis, F. L. (2003). *Aircraft Control and Simulation*. Second Edition, Wiley.
10. Chemezov, D., et al. (2021). Pressure distribution on the surfaces of the NACA 0012 airfoil under conditions of changing the angle of

attack. *ISJ Theoretical & Applied Science, 09 (101)*, 601-606.
11. Chemezov, D., et al. (2021). Stressed state of surfaces of the NACA 0012 airfoil at high angles of attack. *ISJ Theoretical & Applied Science, 10 (102)*, 601-604.
12. Chemezov, D., et al. (2021). Reference data of pressure distribution on the surfaces of airfoils having the names beginning with the letter A (the first part). *ISJ Theoretical & Applied Science, 10 (102)*, 943-958.
13. Chemezov, D., et al. (2021). Reference data of pressure distribution on the surfaces of airfoils having the names beginning with the letter A (the second part). *ISJ Theoretical & Applied Science, 11 (103)*, 656-675.
14. Chemezov, D., et al. (2021). Reference data of pressure distribution on the surfaces of airfoils having the names beginning with the letter B. *ISJ Theoretical & Applied Science, 11 (103)*, 1001-1076.
15. Chemezov, D., et al. (2021). Reference data of pressure distribution on the surfaces of airfoils having the names beginning with the letter C. *ISJ Theoretical & Applied Science, 12 (104)*, 814-844.
16. Chemezov, D., et al. (2021). Reference data of pressure distribution on the surfaces of airfoils having the names beginning with the letter D. *ISJ Theoretical & Applied Science, 12 (104)*, 1244-1274.
17. Chemezov, D., et al. (2022). Reference data of pressure distribution on the surfaces of airfoils (hydrofoils) having the names beginning with the letter E (the first part). *ISJ Theoretical & Applied Science, 01 (105)*, 501-569.
18. Chemezov, D., et al. (2022). Reference data of pressure distribution on the surfaces of airfoils (hydrofoils) having the names beginning with the letter E (the second part). *ISJ Theoretical & Applied Science, 01 (105)*, 601-671.
19. Chemezov, D., et al. (2022). Reference data of pressure distribution on the surfaces of airfoils having the names beginning with the letter F. *ISJ Theoretical & Applied Science, 02 (106)*, 101-135.
20. Chemezov, D., et al. (2022). Reference data of pressure distribution on the surfaces of airfoils having the names beginning with the letter G (the first part). *ISJ Theoretical & Applied Science, 03 (107)*, 701-784.
21. Chemezov, D., et al. (2022). Reference data of pressure distribution on the surfaces of airfoils having the names beginning with the letter G (the second part). *ISJ Theoretical & Applied Science, 03 (107)*, 901-984.
22. Chemezov, D., et al. (2022). Reference data of pressure distribution on the surfaces of airfoils having the names beginning with the letter G (the third part). *ISJ Theoretical & Applied Science, 04 (108)*, 401-484.
23. Chemezov, D., et al. (2022). Reference data of pressure distribution on the surfaces of airfoils having the names beginning with the letter H (the first part). *ISJ Theoretical & Applied Science, 05 (109)*, 201-258.
24. Chemezov, D., et al. (2022). Reference data of pressure distribution on the surfaces of airfoils having the names beginning with the letter H (the second part). *ISJ Theoretical & Applied Science, 05 (109)*, 529-586.
25. Chemezov, D., et al. (2022). Reference data of pressure distribution on the surfaces of airfoils having the names beginning with the letter I. *ISJ Theoretical & Applied Science, 06 (110)*, 1-7.
26. Chemezov, D., et al. (2022). Reference data of pressure distribution on the surfaces of airfoils having the names beginning with the letter J. *ISJ Theoretical & Applied Science, 06 (110)*, 18-25.
27. Chemezov, D., et al. (2022). Reference data of pressure distribution on the surfaces of airfoils having the names beginning with the letter K. *ISJ Theoretical & Applied Science, 07 (111)*, 1-10.
28. Chemezov, D., et al. (2022). Reference data of pressure distribution on the surfaces of airfoils having the names beginning with the letter L. *ISJ Theoretical & Applied Science, 07 (111)*, 101-118.
29. Chemezov, D., et al. (2022). Reference data of pressure distribution on the surfaces of airfoils having the names beginning with the letter M. *ISJ Theoretical & Applied Science, 10 (114)*, 307-392.
30. Chemezov, D., et al. (2022). Reference data of pressure distribution on the surfaces of airfoils having the names beginning with the letter N (the first part). *ISJ Theoretical & Applied Science, 12 (116)*, 801-892.
31. Chemezov, D., et al. (2022). Reference data of pressure distribution on the surfaces of airfoils having the names beginning with the letter N (the second part). *ISJ Theoretical & Applied Science, 12 (116)*, 901-990.
32. Chemezov, D., et al. (2023). Reference data of pressure distribution on the surfaces of airfoils having the names beginning with the letter O. *ISJ Theoretical & Applied Science, 01 (117)*, 624-635.
33. Chemezov, D., et al. (2023). Reference data of pressure distribution on the surfaces of airfoils having the names beginning with the letter P. *ISJ Theoretical & Applied Science, 02 (118)*, 48-61.
34. Chemezov, D., et al. (2023). Reference data of pressure distribution on the surfaces of airfoils having the names beginning with the letter R. *ISJ Theoretical & Applied Science, 03 (119)*, 104-165.

35. Chemezov, D., et al. (2023). Reference data of pressure distribution on the surfaces of airfoils having the names beginning with the letter S (the first part). *ISJ Theoretical & Applied Science, 05 (121),* 331-383.
36. Chemezov, D., et al. (2023). Reference data of pressure distribution on the surfaces of airfoils having the names beginning with the letter S (the second part). *ISJ Theoretical & Applied Science, 05 (121)*, 532-584.
37. Chemezov, D., et al. (2023). Reference data of pressure distribution on the surfaces of airfoils having the names beginning with the letter T. *ISJ Theoretical & Applied Science, 06 (122)*, 28-34.
38. Chemezov, D., et al. (2023). Reference data of pressure distribution on the surfaces of airfoils having the names beginning with the letter U. *ISJ Theoretical & Applied Science, 10 (126)*, 306-327.
39. Chemezov, D., et al. (2023). Reference data of pressure distribution on the surfaces of airfoils having the names beginning with the letter V. *ISJ Theoretical & Applied Science, 10 (126)*, 328-332.